**Peter A. Bandettini, Ph.D.**

# Integration of fMRI Signal Interpretation, Methodology, Technology, and Applications

**Section on Functional Imaging Methods**

**Laboratory of Brain and Cognition, NIMH**

Page

## Introduction – a focus on methods and applications

Over sixteen years ago, the first functional magnetic resonance imaging (fMRI) papers were published. Since then, fMRI has grown in terms of paper publishing rate (now over 2500 papers published a year), range and depth of applications, and sophistication not only of the most advanced fMRI studies but also of the more typical ones. A useful construct is to think of the advancement of fMRI along four inter-related "themes:" Interpretation, Methodology, Technology, and Applications. Interpretation involves understanding the relationship between neuronal activity and fMRI signal changes. Methodology involves the development of techniques to extract and compare this neuronal information. Technology involves the development of hardware, pulse sequences, and new functional contrasts for fMRI. Applications constitute the bulk of published studies that utilize but also drive the development of the other three themes.

When the Unit on Functional Imaging Methods, (UFIM), was established in March of 1999, the goal was to balance the research evenly across the above mentioned themes. The rationale behind this approach was that novel fMRI applications are best carried out by researchers who have an appreciation of the issues involving signal interpretation and an understanding of latest methods and technology. In turn, the most significant advances in fMRI interpretation, methodology, and technology are made by those with their attention focused on applications. UFIM thus recruited individuals with skills that spanned these themes.

Since the last BSC review, UFIM became the Section on Functional Imaging Methods (SFIM) when I received tenure, and the overall research goals have shifted from an even distribution across research themes to more focus on Methodology while maintaining a relatively high number of Applications papers. The emphasis on Methodology reflects what fMRI as a field has been experiencing in recent years. More fMRI publications are deviating from standard procedures involving group comparisons, normalization into a standardized space, and reporting/interpretation of the center of mass of "blobs" of activation. Recently, with advances in techniques such as multivariate analyses "pattern effect mapping," fMRI-based "brain reading", real time fMRI with feedback to the subject, connectivity analysis based on "resting state" fluctuations and diffusion tensor imaging, high field imaging, parallel imaging, the emergence of pulse sequences having novel functional contrast, and high resolution imaging, the field has experienced a healthy resurgence in research effort focused on advancing new techniques rather than applying standard techniques.

The projects of SFIM are integrated across the four themes as the overall goals of our research are: 1) to better understand, extract, and utilize neuronally- related and unrelated signal from time series fluctuations and activation-induced signal changes, 2) to develop and apply an array of methods that make optimal use of high spatial resolution, high sensitivity functional MRI.

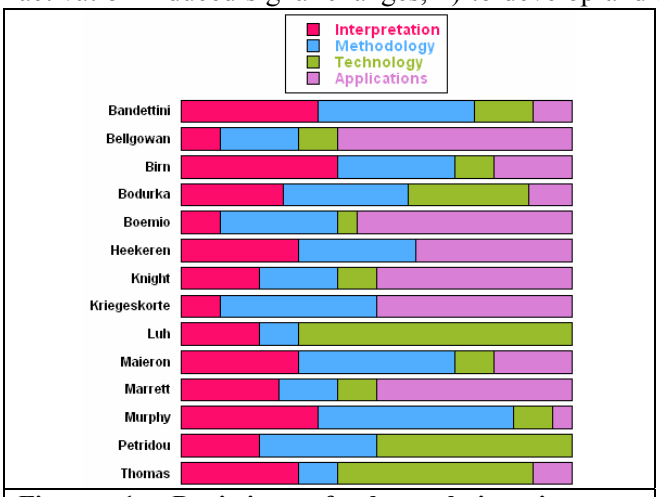


**Figure 1: Depiction of the relative interests (Technology, Methodology, Interpretation, and Applications) of the senior section members (post docs and staff scientists) as well as collaborators over the last four years.**

The goals of SFIM are complementary with those of the functional MRI facility (FMRIF), for which I am also the director. The primary purpose of FMRIF is to provide the most cutting edge fMRI technology for the 25 PIs and total of 250+ NIH researchers who use fMRI. FMRIF strives to put into practical use on the scanners the cutting edge technology and methodology. A fraction of each FMRIF individual's efforts is devoted to research, often in collaboration with members of SFIM. Ideally, FMRIF implements what SFIM develops, and provides the advanced technology on which SFIM relies. Figure 1 shows the individual interests – divided into the four themes - of the SFIM post docs, senior staff, and major collaborators over the last 4 years.

This report is organized in the following manner. The themes are numbered 1 through 4. Within each theme, there are three sub headings: A is the introduction; B is

progress report which describes projects that have been completed in the last four years – most having resulted in published manuscripts; and C describes either unfinished projects – still in abstract form - or planned projects for the following four years. At the introduction to each theme, an overview of the projects will be given. Since 2003, SFIM has published 20 papers and has presented 94 abstracts at scientific meetings. Also, at the end of each project description, the section members and collaborators are listed in parentheses in alphabetical order, with the lead investigator in bold print.

Due to space limitations of this report, all the summaries are brief and many projects summaries have been omitted. Also, while not explicitly mentioned, all future work projects are planned not only for the 3T but also for the 7T scanner operated by Alan Koretsky's Laboratory of Functional and Molecular Imaging (LFMI), thus enabling higher sensitivity, resolution, detectability of physiologic noise, and perhaps unique functional and anatomic contrast.

## Theme 1: Signal Interpretation

### 1A. Introduction: BOLD dynamics and resting state fluctuations

More than four years ago the focus of the Interpretation theme was on better understanding the dynamics of the *activation-induced* fMRI signal change and how it varied over space and with spatial resolution, as well as on the use of this understanding to calibrate the signal or to remove non-neuronally relevant aspects of the signal magnitude and timing. In the past four years, the focus has been redirected, with a similar range of goals, on *time series fluctuations*. Time series fluctuations present a unique challenge in that they contain useful and artifactual information that overlap in spectral power and in space. For detecting activation-related changes, this is less of a concern, but the desire is still to remove these. In the context of extracting useful information from "resting state" time series, the difficulty is high. While some approach the problem with simultaneous measures of neuronal activity (EEG), we have chosen to approach the problem with simultaneous measures of what is presumably the source of the largest and most spectrally-overlapping artifact – changes in breathing depth. Several studies in this theme describe these efforts as well as efforts on identifying other sources of resting state temporal artifacts. An alternative goal in the temporal fluctuation work is the extraction physiologically (but not necessarily neuronally) -relevant information from fMRI time series.

Lastly, in this theme we revisit the issue of understanding the hemodynamic response linearity and our efforts to separate neuronal from hemodynamic sources of these dynamics. This involves probing sources of fMRI non-linearity by task timing modulation and cross-modal comparisons and modeling. Many of the completed studies reported here have been successful continuations of the "current and future" projects that were proposed in the BSC report four years ago.

### 1B. Progress Report

#### 1B-1. The effect of stimulus duty cycle and "off" duration on BOLD response linearity

The BOLD fMRI response has been shown in previous studies to behave in a nonlinear manner, with larger stimuli for brief stimuli than predicted from the response to longer duration stimuli. This nonlinearity can be due either to nonlinearities in the neuronal activity, such as an initial transient increase in neuronal activity, or in a nonlinear dynamic interaction of hemodynamic parameters – the cerebral blood flow, volume, and oxygen extraction. The relative contribution of these mechanisms to the BOLD nonlinearity can be probed by investigating the response to a range of stimulus modulations. Specifically, we investigated the BOLD response to different stimulus duty cycles – a visual stimulus presented either 6% (brief on period), 25%, 50%, 75%, or 94% of the time (brief off period), alternating with a simple fixation control, shown in Figure 2 [1].

In contrast to the BOLD response to brief stimuli, the BOLD response to a brief (1s) cessation of the stimulus, resulted in a smaller decrease than predicted (data not shown) based on a linear extrapolation of longer stimulus

OFF periods. In agreement with this observation, the amplitude of the deconvolved response varied depending on the stimulus duty cycle, with a smaller response for more frequent stimulation.

Possible mechanisms for these nonlinearities were investigated by simulating different neuronal dynamics – transient overshoots in activity following stimulus onsets, a refractory period of this overshoot, and transiently elevated activity following stimulus cessation (an "OFF" response) – as well as different hemodynamics using the balloon model. Figure 3 summarizes these hypotheses.

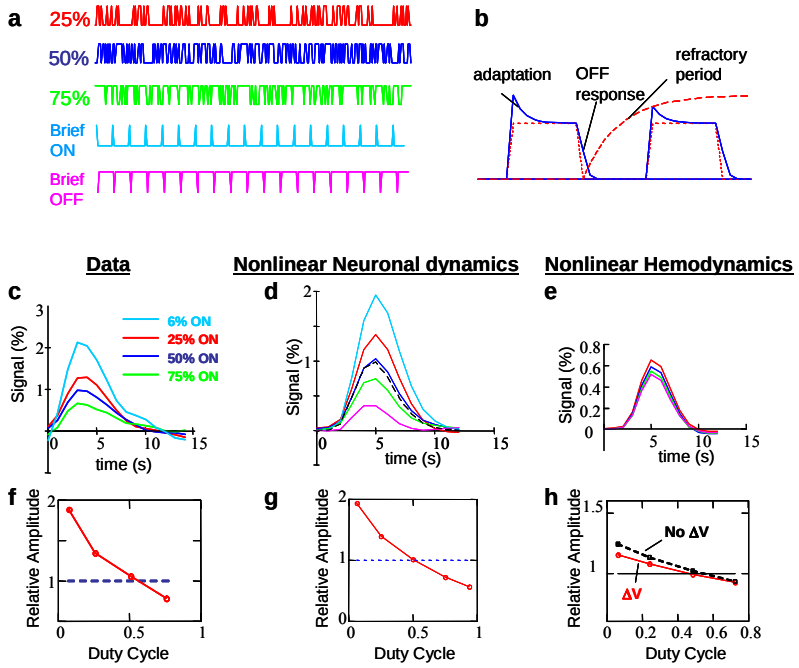


**Figure 2: a: Stimulus timing in which the duty cycle was modulated. b: Schematic illustration of the neuronal mechanism considered: an initial overshoot at the start of stimulation, adapting to a steady state; neuronal firing when the stimulus is turned off; and a refractory period during which the amplitude of the initial overshoot is diminished by closely preceding stimuli. c-e: BOLD response to different duty cycles c. Deconvolved from acquired data, and d-e: from stimulation involving nonlinear neuronal dynamics (d) or nonlinear hemodynamics (e). f-h: relative response amplitude, where 1 indicates a linear response predicting a blocked response. In h., the dashed line indicates the relative amplitudes with no volume changes. The nonlinear hemodynamics cannot account for all the nonlinearity (since it opposes the oxygen extraction nonlinearity effect).**

One hypothesized hemodynamic mechanism for the nonlinearity of the BOLD response to different stimuli durations is a delayed blood volume response [2, 3]. An elevated blood volume by itself causes a decreased BOLD signal. If the blood volume changes significantly only for longer duration stimuli, then shorter duration stimuli will result in a slightly larger response (i.e. signal reducing blood volume effect lags behind). However, most models also predict an elevated blood volume for a period following the cessation of a stimulus. This would predict a larger than linearly proportional decrease for brief stimulus OFF periods compared to longer stimulus OFF periods, *opposite to what has been observed here*. The only hemodynamic nonlinearity that can therefore account for the observed response to stimulus cessations is a nonlinear relationship between the oxygen extraction and blood flow. Our models show that for physiologically realistic parameters, this can only account for up to half of the observed nonlinearity. In contrast, the nonlinear neuronal dynamics could by itself explain most of the nonlinearity in the BOLD response. This suggests that the BOLD response reflects, to some degree, the neuronal dynamics, although one can't completely rule out hemodynamic contributions. (**Birn**)

## 1B-2. Linearity of the BOLD response to ramped stimuli – comparison with MEG

Previous studies have shown that the BOLD fMRI response behaves in a nonlinear manner for brief stimuli (< 2s duration), with a larger response than expected based on the response to longer duration stimuli. As mentioned in 1B-1, nonlinearity could result from a nonlinear interaction of the dynamics of cerebral blood flow, cerebral blood volume, and oxygen extraction. Alternatively, the nonlinearity could result from a transient overshoot in neuronal activity when the stimulus is first presented. In this study, we investigated the role of these neuronal transients by varying the rate at which the stimulus contrast of the visual stimulus is increased. A contrast reversing checkerboard was presented either with an abrupt transition in contrast, or with a more gradual increase (and decrease) over a period of either 0.5s or 1s. Stimuli were presented in a slow

event-related design, once every 15s. In addition, the neuronal activity evoked by these stimuli was investigated in a separate experiment using magnetoencephalography (MEG).

Using a ramped stimulus contrast onset successfully caused a reduction in the transient overshoot in neuronal activity (as measured by the total MEG power across all frequencies) relative to the steady state, but the neuronal activity increased nonlinearly with the ramped increase in stimulus contrast, effectively lengthening the stimulus duration. This resulted in a slight nonlinearity of BOLD responses predicted from the MEG response to different stimulus durations for all ramp durations (see Figure 3b). This nonlinearity, however, was much smaller than the observed BOLD response nonlinearity (see Figure 3a). This suggests that the fMRI BOLD nonlinearity is not solely due to this transient neuronal activity. Future work will involve verification of these findings using better defined and understood stimuli. (Birn, **Tuan**)

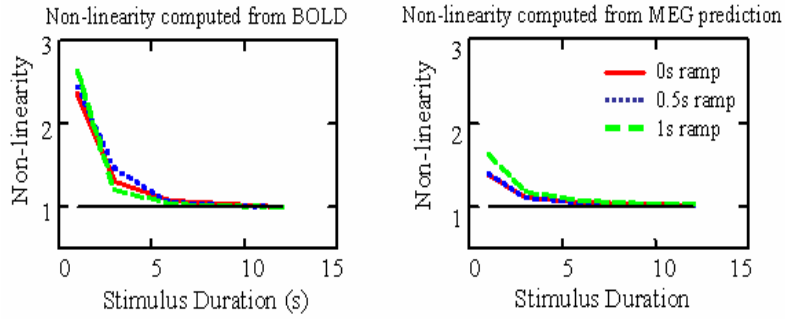


a b

**Figure 3: Non-linearity with varying onset ramp durations, relative to steady state blocked signal amplitude, of a. BOLD signal, and b. MEG-predicted BOLD signal assuming a linear relationship between MEG and BOLD signal. While some nonlinearity is predicted by MEG, not all of it is explained, suggesting that BOTH hemodynamics and neuronal activity contribute to BOLD nonlinearities.**

## 1B-3. The effect of respiration changes on fMRI measures of activation and connectivity

The goals of this study [4] were: 1) to characterize the temporal and spatial patterns of fMRI signal changes that are induced by variations in respiration; 2) to investigate the impact of these respiration variations on analyses of task-related activation and for resting-state functional connectivity; and 3) to evaluate methods to reduce the respiration artifact. A method is also introduced by which these variations in respiration can be estimated from a respiration belt placed around the subject's chest without the need for a separate monitor for end-tidal $CO_2$.

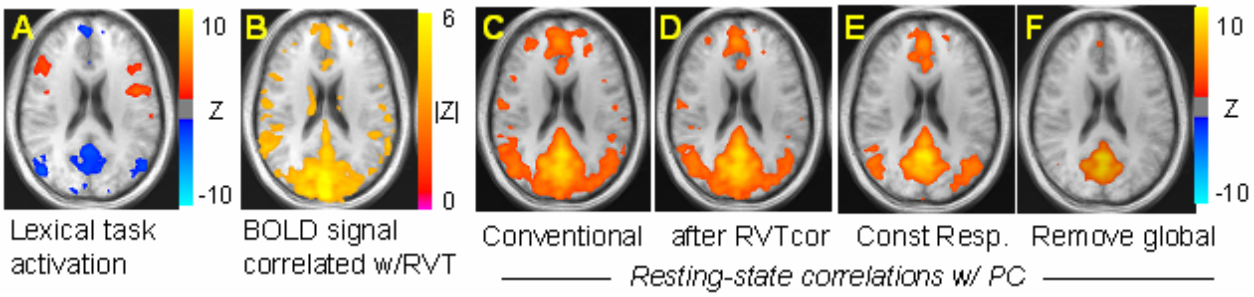


**Figure 4: A) Activations (red) and deactivations (blue) during a lexical decision making task; B) fMRI signals correlated with changes in respiration volume per time (RVT); C-F) Voxels correlated with the posterior cingulate (PC) at rest: C) with conventional connectivity analysis using RETROICOR [5] to correct for physiological noise; D) correlations after regressing out RVT changes (RVTcor); E) correlations during cued constant respirations; F) correlations after regressing out global signal changes.**

Figure 4 shows that the signal changes related to *changes* in respiration (as opposed to the respiration cycle itself) were found to overlap with many of the areas identified as part of the 'default mode' network. This is certainly of concern with regard to the interpretation resting-state functional connectivity data. Monitoring and removing these respiration variations led to a significant improvement in the identification of task-related activation and deactivation, but only a moderate change in a functional connectivity results. We are still investigating the limited success of this approach to the resting state results. Regressing out global signal

changes, or cueing the subject to breathe at a constant rate and depth resulted in an improved spatial overlap between deactivations and resting state correlations. (**Birn**, Diamond, Jones, Smith)

### 1B-4. The respiration response function

Changes in the subject's breathing rate or depth, such as a breath-hold challenge, can cause significant fMRI signal changes throughout gray matter, CSF, and cerebral blood vessels. However, the response function that best models breath-holding induced signal changes, as well as those resulting from a wider range of breathing variations including those occurring during rest, has not yet been determined.

These signal changes are slower than neuronally induced BOLD signal changes, and cannot be modeled using the brain activation-induced hemodynamic response function. The goal of this study was to derive a new response function that can be used to model fMRI signal changes induced by variations in the respiration volume. This "respiration response function," as shown in Figure 5a., was determined by averaging the response to a series of single deep breaths performed once every 40s amongst otherwise constant breathing.

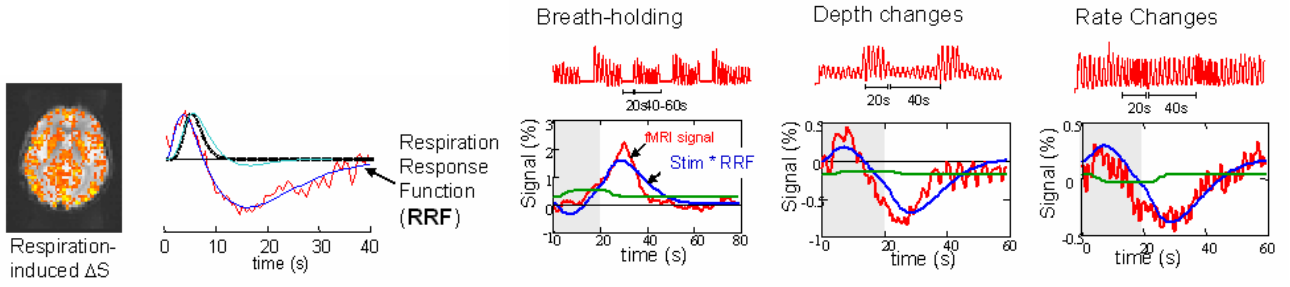


**a.** **b.**

**Figure 5: a. Respiration-induced signal changes in response to a deep breath. Image show areas that are significantly correlated with this function. Red curve: Impulse response function derived from a Wiener deconvolution of the averages response to a single deep breath. Dark blue curve: ideal fit representing the Respiration Response Function. Dotted line shows the typical gamma-variate HRF typically used to model activation induced BOLD changes. The light-blue line shows the canonical HRF used on SPM, based on a difference of two gamma-variate functions. b. Averaged fMRI responses to respiration modulations: Breath-holding, cued depth changes, and cued rate changes. Blue curves: fit of RVT convolved with respiration response function. Green curve: fit of RVT convolved with typical Gamma-variate used for BOLD responses. Responses are averaged across 11 subjects.**

This average response is characterized by an early signal increase (earlier than the activation-induced signal change) followed by a later and highly pronounced undershoot that shows a minimum at approximately 16s. When convolved with the breath-to-breath changes in respiration volume, this response function accurately models the fMRI signal changes that result from the cued breath holding as well as cued depth and rate changes, as shown in Figure 5b. (**Birn**, Jones, Smith)

### 1B-5. Artifactual, adjacent-voxel time series correlations in echo-planar data

Another potential source of artifact when performing voxel-wise correlations on resting state data is that of the correlations between adjacent voxels that arises from a combination of scanner instability and the unavoidable reality of shared signal power between adjacent MRI voxels (adjacent voxels share signal power is under an envelope approximating a sinc pulse). This may be a source of local correlations that have been interpreted as due to highly local functional connectivity [6]. We demonstrated this local spatial correlation by showing the time-course correlation as a function of voxel separation within and across slices for a human brain in resting state and for a water-filled sphere (phantom). The plots of adjacent voxel correlation as function of spatial separation from human brain and phantom time series, shown in Figure 6, are surprisingly similar. Both show correlations that extend further than with the signal taken from the areas of no signal. The spatial correlation structure found in the phantom must be artifactual. Artifactual correlations spanning up to two centimeters occur within and between different imaging slices. (Bodurka, **Kriegeskorte**)

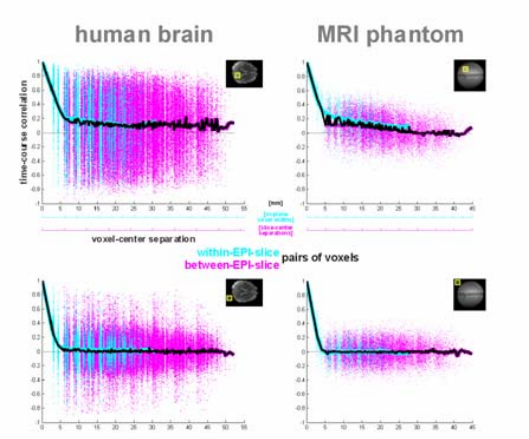


**Figure 6: fMRI time-course correlation between voxels. Linear correlation between the voxel time courses as a function of the distance between the voxels for the human brain in resting state (left) and an MRI phantom (right). Each pair of voxels is represented by a dot (cyan if the voxels are from the same slice, magenta otherwise). The average correlation functions are plotted as solid lines (black for all voxel pairs, cyan for within-slice voxel pairs, magenta for between-slice voxel pairs). X-axis units are mm. These analyses were performed for cubic regions of interest of 8×8×8 voxels located either inside (top) or outside the object (bottom).**

## 1C. Current and Future Experiments

### 1C-1. Echo time dependence of physiologic noise.

Krueger et al. have introduced a model in which physiological noise is divided into BOLD and non-BOLD related components [7]. By separating the fluctuations that are echo time (TE) dependent from those that are not, one should be able to cleanly separate susceptibility-related from non-susceptibility related (and therefore, optimistically, non-neuronal) fluctuations. We investigate this technique further by characterizing the time series power spectrum of the TE dependent signal changes.

Six resting-state runs with varying flip angles were collected using a GE-EPI sequence while recording physiological traces with a pulse oximeter and a respiration belt (n=4). By varying the flip angle across runs, the Krueger model can be fitted to the data and an estimate of $\lambda$ (which describes the relative proportion of physiologic noise) can be obtained. This $\lambda$ can be written in terms of BOLD and non-BOLD noise contributions, $\sigma_B$ and $\sigma_{NB}$ respectively, where is $\sigma_B$ isTE dependent and $\sigma_{NB}$ is not. By collecting multi-echo data, the TE-dependent term, $\sigma_B$, can be cleanly separated from the remaining noise contributions. Multi-echo acquisition has the added advantage of allowing calculation of $T_2$* and $M_0$ time series by fitting $S=M_0\exp(-TE/T_2^*)$ to the five TE values. Imaging parameters: Axial plane, 3 slices, 24cm FOV, 5mm slice thickness, Matrix size = 32 x 32, TR=350ms, TE=17, 37, 57, 77 and 97ms, flip angles 45, 36, 27, 18, 9 and 0 degrees, number of repetitions=700.

The TE-dependence of $\sigma_B$ scaled to $\sigma_0$ is shown in Figure 7a and confirms the inverted U-shape presented in original Krueger study. After calculating the power spectrum density (PSD) at each TE, shown in Figure 7b, correlations of this inverted U-shape with the power at each frequency across TE allows us to determine which frequencies display the greatest TE-dependence and thus the greatest susceptibility-related fluctuations.

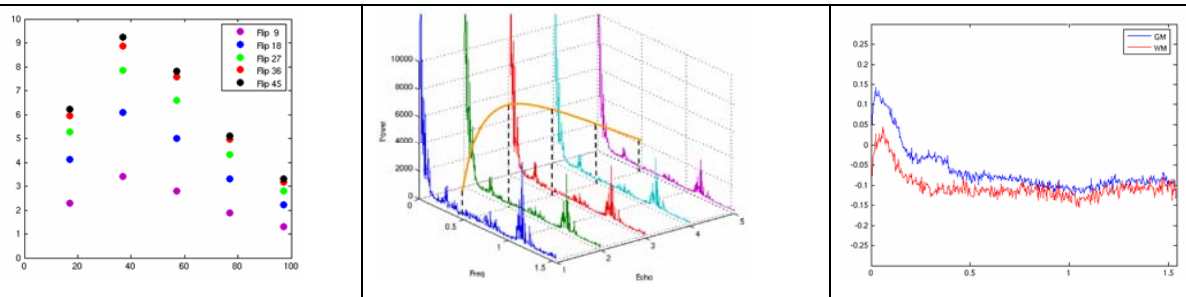


**a** **b** **c**

**Figure 7: a. TE-dependence of $\sigma_B$ scaled to $\sigma_0$ is shown in grey matter for varying flip angles. b. Illustration showing that a fit of $\sigma_B$ from the Kruger model was carried out on the power spectrum density (PSD) across 5 echoes. This was the procedure by which c. was created. c. The frequency profile of TE-dependent fluctuations. The x-axis units for b and c are Hz. The x-axis units are ms.**

Figure 7c shows this correlation averaged over all flip angles and subjects, demonstrating that: 1) TE-dependent fluctuations are predominantly at lower frequencies (<0.1Hz), 2) gray matter exhibits higher BOLD related fluctuations than white matter suggesting either a difference in vasculature and/or the presence of fluctuations related to neuronal firing and 3) there exists an increase in TE-dependent noise around the breathing frequency (~0.3Hz), which may reflect neuronal or non-neuronal susceptibility-related changes. An alternative way to analyze this data is by observing the difference in the power spectra of the $T_2$* and $M_0$ time series. Since BOLD related fluctuations should affect T2* and not $M_0$, this difference will determine at what frequencies these fluctuations are present. This avoids some errors that may occur in fitting of the data as $M_0$ changes may cause a similar change to artifactually appear in T2*. Taking the difference in these measures reduces these errors.

It is clear that there exist noise sources in the data that are TE-dependent but not related to neuronal activity. These physiological noise sources can be removed from the data using standard methods such as RETROICOR [5]. However, there exist other physiological noise sources that are low-frequency and TE-dependent such as changes in breathing depth over time. These changes produce fluctuations at ~0.03Hz and can be removed by RVT correction. After removing these, well-defined TE-dependent peaks are present at low frequencies (<0.1Hz) whose sources appear to be distributed across the entire brain.

The question of whether neuronally-related BOLD fluctuations can be cleanly separated from other sources of noise is unresolved. This study demonstrates that limiting analysis to the lower frequencies is not enough. By also adding the constraint of TE-dependence, one still has to be concerned with correction of low-frequency physiological noise components. So, while multi-echo data combined with Fourier analysis is a potentially useful tool, it does not completely separate neuronally from non-neuronally related BOLD fluctuations. Combined with physiologic correction techniques, multi-echo data may prove to be more useful than the physiologic correction techniques alone. (Birn, Bodurka, Luh, **Murphy**)

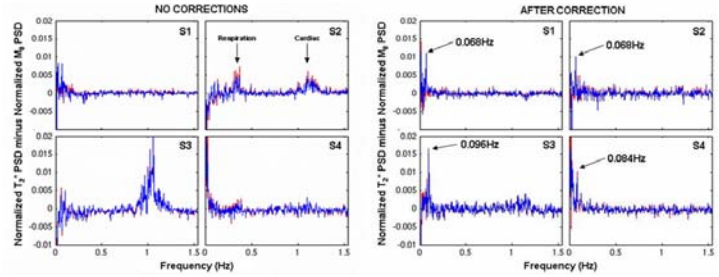


**Figure 8: The difference of the $T_2$* and $M_0$ PSD curves are shown for each subject without and with physiologic correction. Physiologic noise manifests itself in the $T_2$* PSD, but, after physiologic correction, breathing (0.35Hz), cardiac (1.1Hz), and lower (~0.03Hz) frequencies, related to RVT, are removed. All subjects show TE-dependent peaks at ~0.1Hz.**

## 1C-2. Sensitivity of BOLD contrast to neuronal firing rate vs. number of active neurons

An open question regarding BOLD contrast concerns precisely how it reflects neuronal activity. Does it matter how neuronal activity is temporally and spatially integrated within a voxel in the time scale of the hemodynamic response? Given a constant integrated neuronal activity, do many neurons firing infrequently elicit a different BOLD response than a few neurons firing rapidly? In this study, the central issue is not whether or not local field potentials or spiking influence BOLD changes since we assume that for these particular stimuli, changes in local field potentials and spiking rates that correspond to changes in the stimuli parameters are proportional to each other.

Some studies report linear increases in BOLD-signal in human MT (hMT+) with increasing stimulus coherence in random dot displays[8, 9]. This is interpreted as evidence for a linear relationship between non-simultaneous measures of neuronal firing rate and hemodynamic changes[8]. Other studies, however, found higher activity in hMT+ in response to incoherent motion compared with coherent motion[10]or no difference at all[11].

To test how motion coherence modulates the BOLD response in hMT+ and other areas, we used a blocked design fMRI study in which subjects viewed a random dot display for 1s and decided whether the stimulus was moving to the left or to the right. Coherence varied randomly from block to block (0%, 6.4%, 12.8%, 25.6% and 51.2%). hMT+ was identified independently, in Figure 9a, using a low contrast motion stimulus. Shown in Figure 9b is the response magnitude from this region as a function of stimulus contrast.

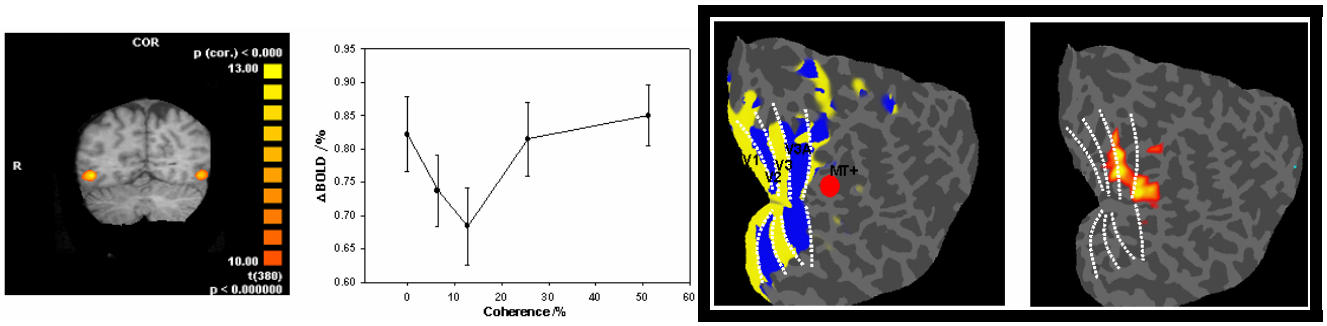


**a.** **b.** **c.**

**Figure 9. a. hMT+ localized with a low-contrast moving stimulus. b. BOLD signal change in hMT+ as a function of coherence (N=6). Note the non-monotonicity of the curve. c. Retinotopic areas and result of group analysis using a U-shaped reference function displayed on the flattened occipital cortex of one subject. Note the main foci in V3/V3A and hMT+.**

In a second blocked design fMRI experiment, we tested whether the non-monotonic shape of the BOLD response was due to attentional effects. In addition to the random dot stimulus, the letters L and T were flashed rapidly (5Hz) at fixation. Before each block the subjects were cued to either do the letter discrimination task (count the number of Ls or Ts, LETT) or the motion discrimination task (MOT). When subjects performed LETT the BOLD response in hMT+ was smaller than during MOT; the shape of the BOLD response as a function of coherence, however, was U-shaped in both experiments. Thus it is unlikely that the non-monotonicity in the BOLD-response is due to attentional modulatory effects.

These data are consistent with a recent study reporting that in anesthetized monkeys BOLD signal varied non-monotonically as a function of noise in visual stimuli[12], supporting the view that BOLD-contrast measures a heterogeneous pooled neural response. According to this view, at 0% coherence (pure noise) many weakly activated neurons with different preferred directions would cause a similar summed BOLD response as few highly active neurons at 51.2% coherence tuned to that direction.

To test the this model directly, we are using motion stimuli with which we modulate separately the firing rate and the number of active neurons by parametric manipulations of the number of dots, their coherence, and velocity. According to this model, shown in Figure 10, we predict that BOLD contrast change corresponding to changes in either firing rate or to the number of active neurons will be more rapid than the other, thus summing to cause the observed dip in BOLD response at 12% contrast. (Boemio, Heekeren, Kriegeskorte, **Marrett**, Murphy, Parr, Ruff)

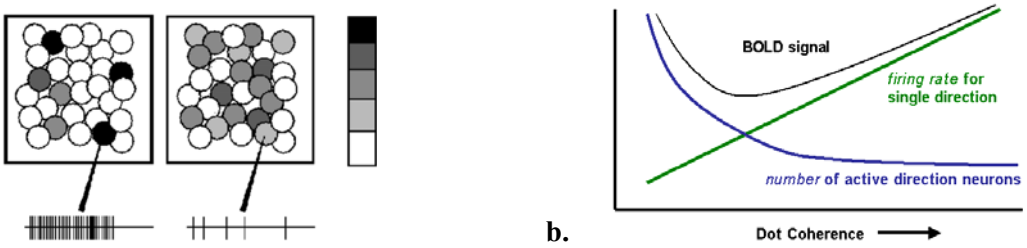


**a.** **b.**

**Figure 10.a. Contribution of number of neurons firing and firing strength to summed population response (adopted from [12]). B. Hypothesized component contributions to BOLD signal and their subsequent summation to produce the curve in Figure 9.**

## Theme 2: Methodology

### 2A. Introduction: An increased role of methodology advancement

As mentioned, fMRI has been experiencing an increased focus on methodology development. Specifically, researchers are looking much closer at time series fluctuations, calibration techniques, voxel-wise patterns of activation, and the modulation of activation by real time feedback to the subject. This research is the most active area of our group. Specifically, we have been focusing on methods to remove unwanted fluctuations from fMRI time series as well as to calibrate the time series signal such that neuronal activity during "rest" and activation may be accurately assessed, mapped, and compared. We have also been focusing on methods to make use of the information contained in voxel-wise patterns of activation rather than mapping of activation areas. Lastly, we've been working on straightforward, yet practical issues of what determines the optimal resolution at which to scan, and how long one needs to scan.

### 2B. Progress Report

#### 2B-1. Analyzing for information, not activation, to exploit hi-res fMRI.

*Challenges of hi-res fMRI*

High-resolution functional magnetic resonance imaging (hi-res fMRI) promises to help bridge the gap between the macro- and the microview of brain function afforded by conventional neuroimaging and invasive cell recording, respectively[13]. Hi-res fMRI (voxel volume $\leq (2\ \text{mm})^3$ ) is robustly achievable in human studies today using widely available clinical 3-Tesla scanners. However, the neuroscientific exploitation of the greater spatial detail poses four challenges (Fig. 11): (1) Hi-res fMRI may give inaccurate (i.e. blurred, displaced and distorted) images of fine-scale neuronal activity patterns. (2) Single small voxels yield very noisy measurements. (3) The greater number of voxels complicates interpretation and poses a more severe multiple-comparisons problem. (4) The functional correspondency mapping between individual brains is unknown at the fine scale of millimeters. These challenges can be met by shifting the focus of brain mapping and region-of-interest analysis from the activity patterns to the amount of information they convey about experimental conditions. Multivoxel-pattern-recognition analysis of regions of interest reveals such information. We introduced two related developments: (1) A method for continuous mapping of local pattern information using a multivariate searchlight (below) and (2) representational similarity analysis(discussed in 4C-2).

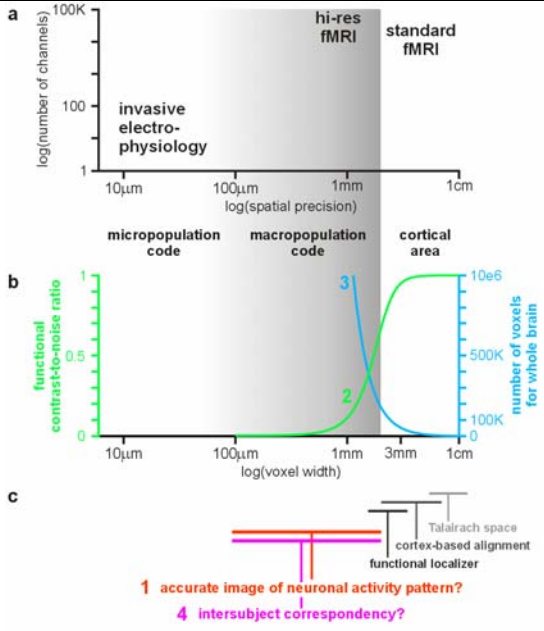


**Fig. 11: Four challenges of hi-res fMRI. a. Comparison of fMRI (standard and hi-res) and invasive electrophysiology in terms of spatial precision and number of channels, with which brain activity is simultaneously measured. The grey shading indicates the precision range of hi-res fMRI (≤ 2 mm voxel width). b. The FCNR drops rapidly when fMRI resolution is increased (challenge (2), green). The blue curve shows the rapid growth of the number of voxels needed to cover the brain as voxels become smaller (challenge (3), blue). c. In the hi-res range (gray shading), fMRI may give an inaccurate (blurred, distorted, displaced) image of the neuronal activity pattern (challenge (1), red). Moreover, a voxel-to-voxel intersubject correspondency is very difficult to define and, in fact, may not exist (challenge (4), magenta). Standard fMRI, by contrast, operates at the spatial scale of cortical areas. At this coarser scale, hemodynamic blurring, distortion and displacement of neuronal activity patterns is less problematic and intersubject correspondency is roughly determined by the Talairach common space.**

*Information-based searchlight mapping*

Brain mapping analysis has focused on the discovery of *activations*, i.e. of extended brain regions whose *average activity* changes across experimental conditions. Here we propose to ask a more general question of the data: Where in the brain does the activity *pattern* contain *information* about the experimental conditions? To address this question we combine classical brain mapping with multivoxel pattern-information analysis [14].

The information in local contiguous activity patterns is mapped out by scanning the imaged volume with a spherical "searchlight", whose contents are analyzed multivariately at each location in the brain. All the steps of this technique are shown in Figure 12. (**Kriegeskorte**)

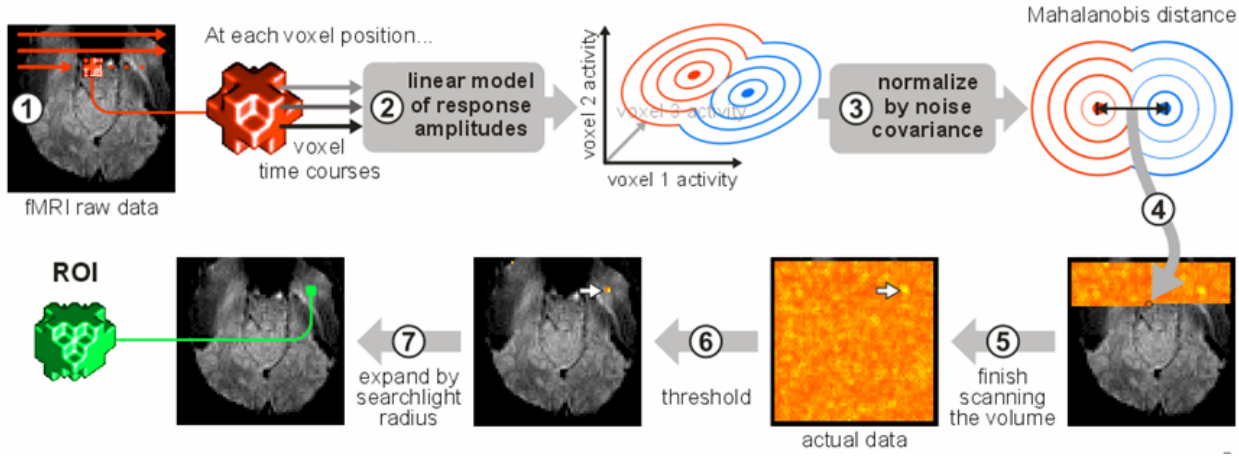


**Figure 12: Searchlight procedure: In order to find regions whose response pattern distinguishes two conditions, the imaging volume is scanned with a spherical multivariate searchlight (1, red voxel cluster). The searchlight is centered on each voxel in turn (selecting overlapping voxel sets at adjacent positions). For each voxel position, the time courses of all voxels falling within the searchlight are subjected to joint multivariate analysis (2, 3). As a measure of response-pattern difference, we use the Mahalanobis distance. The Mahalanobis distance representing the response-pattern difference within the searchlight is recorded in a map at the central voxel position (4). The whole volume is scanned in this manner (5). Note that the resulting map represents local response pattern information, not activation. The map (between steps 5 and 6) shows actual data from a single subject viewing face images. The white arrow marks the map maximum. The map is thresholded (6) to define the region distinguishing the two conditions. Optionally, the highlighted voxel cluster can be expanded by the searchlight radius (7), in order to obtain an ROI that includes all voxels that contributed to the local multivariate effects indicated by the super-threshold voxels. The location and shape of the region thus defined represents a subject-specific hypothesis, which is subsequently tested on independent data. Statistical inference can alternatively be performed on whole information-based maps by randomization of the condition labels.**

## 2B-2. Determination of the "suggested" fMRI resolution.

This work addresses the choice of the imaging voxel volume in blood oxygen level dependent (BOLD) functional magnetic resonance imaging (fMRI) [15]. Noise of physiological origin that is present in the voxel time course is a prohibitive factor in the detection of small activation-induced BOLD signal changes. If the physiological noise contribution dominates over the temporal fluctuation contribution in the imaging voxel, further increases in the voxel signal-to-noise ratio (SNR) will have diminished corresponding increases in temporal signal-to-noise (TSNR), resulting in reduced corresponding increases in the ability to detect activation induced signal changes. On the other hand, if the thermal and system noise dominate (suggesting a relatively low SNR) further decreases in SNR can prohibit detection of activation-induced signal changes. Here we have proposed a "suggested" fMRI voxel volume where thermal plus system-related and physiological noise variances are equal. This is concept is illustrated in Figure 13.

Based on this condition we have created maps of fMRI suggested voxel volume from our experimental data at 3T, since this value will spatially vary depending on the contribution of physiologic noise in each voxel. Based

on our fast EPI segmentation technique we have found that for grey matter (GM), white matter (WM), and cerebral spinal fluid (CSF) brain compartments the mean suggested cubical voxel volume is 1.8 $mm^3$, 2.1 $mm^3$ and 1.4 $mm^3$, respectively. Serendipitously, 1.8 $mm^3$ voxel volume for GM approximately matches the cortical thickness, thus optimizing BOLD contrast by minimizing partial volume averaging. (**Bodurka**, Murphy, Petridou, Ye)

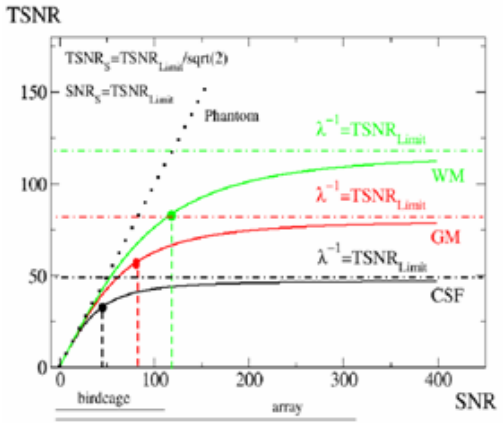


**Figure 13: A simulation of the TSNR versus SNR relationship for three different brain tissue components and a phantom. The lines represent the human brain white matter (green), gray matter (red), and cerbro-spinal fluid (black). The dark dotted line represents the expected result for a phantom (no physiological noise present). The locations of the suggested voxels for specific brain compartments where Eq. (2) holds are marked using large color dots. The dashed vertical lines indicate TSNR and SNR coordinates for SVV and the horizontal dotted/dashed lines limit for TSNR. The black horizontal lines below the horizontal axis show the SNR range available with the system standard transmit/receive birdcage coil and the 16 channel receive-only surface coil brain array are used.**

### 2B-3. Design and processing strategies for overt responses

In the previous BSC report we demonstrated, using simulations in the "current and future experiments" section, that task-related motion artifacts during overt speech can be reduced by using specific stimulus timings, such as event-related designs or even a blocked design with a 10s block duration alternated with a 10s rest period. These designs exploit the differences in the temporal characteristics between the rapid motion-induced and the slower hemodynamic signal changes. In a continuation of this initial study, we evaluated various event-related and blocked designs involving overt word reading in their ability to detect function and to avoid speech-induced motion artifact, using both simulation and experiments [16]. A blocked design with task and control durations of 10s, and an event-related design with a minimum stimulus duration of 5s and an average inter-stimulus interval of 10s were found to optimally detect blood oxygenation level dependent signal changes without significant motion artifact. These results are demonstrated experimentally in Figure 14.

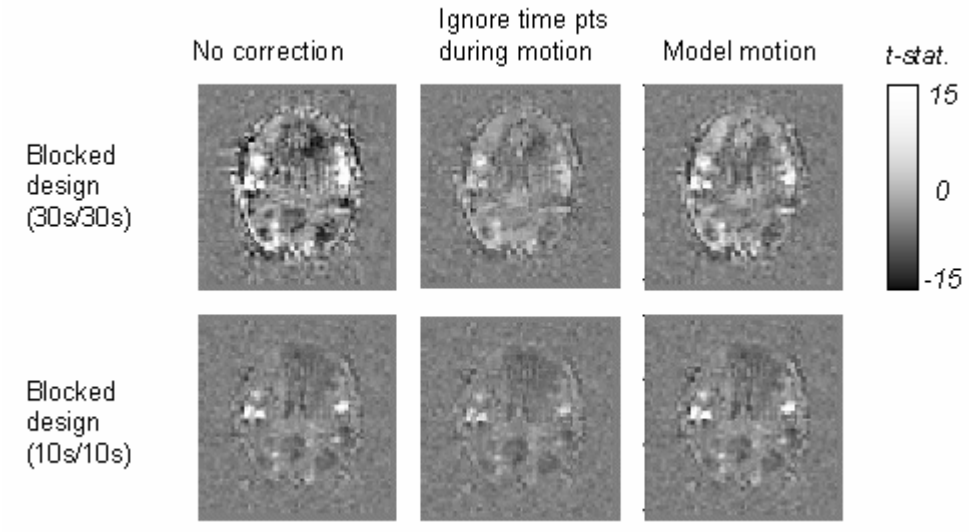


**Figure 14: One axial brain slice at the level of the motor cortex showing the t-statistic maps of the correlation of an ideal BOLD response for blocked design with two designs: 30s task/30s control, and 10s task/10s control. Three analysis strategies are shown: (left) no correction for task-related motion (aside from registration), (middle) ignoring time points during the task, (right) and using the task timing to model the motion-induced signal change.**

Ignoring images acquired during speech can help recover signal in areas affected by motion, but substantially reduces the detection power in other regions. Using the stimulus timing as an additional regressor to model the motion offers little benefit in practice, due to the variability of the motion induced signal change.

In addition, these methods were applied in our collaboration with Alex Martin in his studies involving patients with autistic spectrum disorder as they produced overt verbal responses. Also, as described in 4C-1, we apply this technique in normal subjects as they performed a verbal fluency task. (**Birn**)

### 2B-4. Determining the minimally necessary scan duration.

Noise in fMRI data necessitates signal averaging to extract functional signal changes. This noise has physiological and scanner-related contributions and is a major obstacle to detecting activation in a single time series. The relative fraction of physiologic noise increases linearly as a function of SNR, hence as image SNR increases, temporal signal to noise ratio (TSNR) in oxygenation-sensitive BOLD signal saturates.

A natural development in fMRI is a progression towards high spatial resolution. To investigate small-scale structures of ~1mm$^3$ size that exist in the brain such as cortical layers and columns, detection of activation in high-resolution single voxel time series is required, and multi-subject averaging is prohibitively difficult. This study characterizes the relationship between TSNR and the necessary scan duration to reliably detect activation in a single voxel with a given fractional signal change[17]. Using standard equations for *TSNR*, correlation coefficient (*cc*) and *P* value as it relates to *cc* and assuming that an fMRI time series contains block activations with an effect size *eff*, we were able to derive an equation that calculates the number of time points required to detect the activation: $N = 8\left(\frac{erfc^{-1}(P)}{(TSNR)(eff)}\right)^2$

Simulations using 600,000 of fMRI time series with a Gaussian noise distribution were used to verify the validity of the theory. A good correspondence with the theory was found with only slight discrepancies when detecting small effect sizes at very strict *P* values. The simulations allowed us to determine a new measure, $TSNR_G$, which was defined as the TSNR level that guarantees detection. Figure 15a shows the difference between this measure and the theory.

Both the theory and simulations assume that noise in fMRI data is Gaussian, and each time point is independent. Physiological noise, though, is not Gaussian and introduces autocorrelations into the data that can disrupt the ability to detect activations. Resting state data was acquired from 5 subjects to determine the legitimacy of the $TSNR_G$ measure. When using this noise containing autocorrelations, a far greater number of time points are required to detect activation. However, at high resolution (low SNR), physiological noise contributions are reduced and hence the results from the resting state data correspond more closely to the simulated results, shown in Figure 15b. It has been shown that the $TSNR_G$ measure derived from the simulations is valid in the high resolution fMRI regime. An equation that determines the number of time points required to guarantee activation detection was derived by modifying the theory above using non-linear fitting techniques: $N_G = 8\left[1.5\left(1+e^{\log_{10} P/2}\right)\left(\frac{erfc^{-1}(P)}{(TSNR)(eff)}\right)\right]^2$. This equation is plotted in Figure 15c and demonstrates that if the goal is to image at columnar resolution (~1.5mm$^3$) with an effect size of 1% at 3T using standard techniques, doubling the TSNR can decrease the required experimental length four fold. It also show that at typical SNR values, obtaining significant results under these constraints will require over 2000 time points. (Bodurka, **Murphy**)

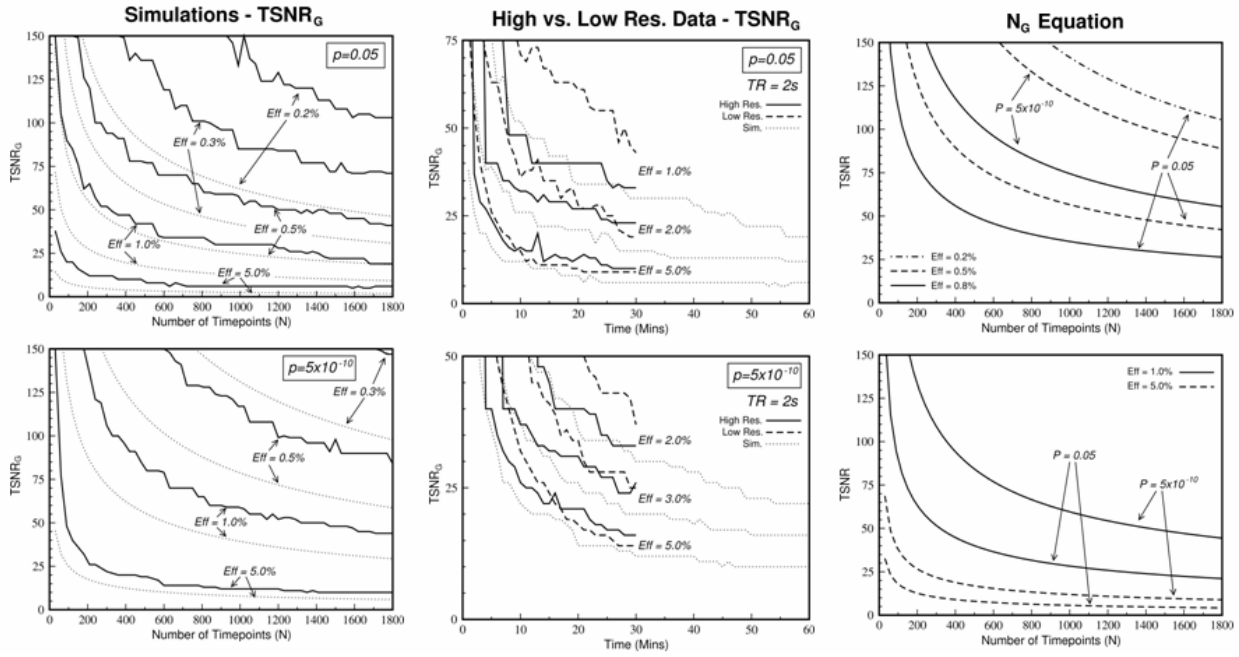


**Figure 15: a. The TSNR values that guarantee activation (TSNR$_G$) according to the simulations are shown with the solid line. The corresponding theoretical curves are shown with dotted lines. Simulated TSNR$_G$ values are greatly elevated above the theoretically derived values. b. The effect of removing most of the physiologic noise by increasing the resolution can be seen. By removing physiologic noise, the datasets become more Gaussian and therefore more like the simulated curves, especially at smaller effect sizes and lower scan durations. Hence, if the influence of physiological noise can be removed by using methods such as RETROICOR, pre-whitening and higher resolution scans, the simulated data give the true relationship between required TSNR and require scan duration. c. The TSNR$_G$ values derived from the simulations can be used as a gold standard for determining the required scan duration for detecting activation. Plots of the equation (in text) that fit these data are shown for various effect sizes and *P* values. When acquiring in the high-resolution regime, where physiological noise is reduced and the remaining noise is close to Gaussian, these graphs can be used to determine the number of time points required to detect the activation. For example, to detect an effect size of 1.0%, to a liberal threshold of *P* = 0.05 when the TSNR=50, ~320 time points are required but to detect activation with a conservative threshold of *P* = 5x10-10 nearly 1500 time points are required.**

## 2C. Current and Future Experiments

### 2C-1. Calibration of BOLD signal change with cued or spontaneous breathing variations

The amplitude of the BOLD response depends strongly on the underlying vasculature, with the largest responses generally occurring in large draining veins. This heavy vascular, or resting venous blood volume, weighting makes it difficult to determine subtle differences in the amount of neuronal activity between brain regions or between subjects. Earlier studies have suggested calibrating the BOLD signal by using a hypercapnic challenge, achieved either by an administration of $CO_2$ or by breath-holding. This can provide a map of the relative changes in signal from a global and presumably uniform increase in blood flow [18-20]. Here we show that a similar calibration of the BOLD response can be obtained by having the subject perform cued breathing depth or rate changes, or by measuring normal, spontaneous variations in breathing during rest.

Eleven subjects each performed 6 runs – 1) viewing a contrast-reversing checkerboard alternated with a gray fixation screen (blocked design), 2) resting with eyes closed, and performing various cued breathing manipulations: 3) breath-holding, 4) depth changes, 5) rate changes, 6) a single deep breath every 60s. Heart rate and respiration were recorded with a pulse oximeter and a pneumatic belt, respectively. Respiration volume per time (RVT) changes were estimated by dividing the difference between the maximum and minimum belt positions (the respiration volume) by the time between breaths (the respiration period) [4].

A response function to model respiration induced changes was determined from the average response to the single deep breath. This was convolved with the RVT changes and fit to the signal changes in the other tasks. For both task- and respiration-related analyses the regression was repeated with different temporal shifts of the ideal response, and the latency that gave the best fit was used in each voxel. Task-induced and respiration-induced signal changes were compared, and a calibrated BOLD response was produced by dividing the task response amplitude by the normalized respiration response amplitude.

Figure 16 shows that the amplitude of the task-induced BOLD response across the activated region of the visual cortex significantly correlated with the respiration-induced signal changes during breath-holding, as well as cued depth changes, rate changes, and natural changes in respiration depth and rate during rest. Respiration-induced signal fluctuations during rest were of the same magnitude, and in some cases larger, than breath-holding induced changes. Calibration of the task-induced BOLD fMRI response, which was similar for all breathing manipulations, shifted the peak of the visual activation from voxels near the sagittal sinus to more lateral and medial cortical regions. Resting scans, or a wider range of breathing manipulations, can be performed more easily than an administration of $CO_2$ or breath-holding, and can therefore enable the application of calibration across a wider range of subjects and patient groups. (**Birn**, Handwerker, Jones, Murphy)

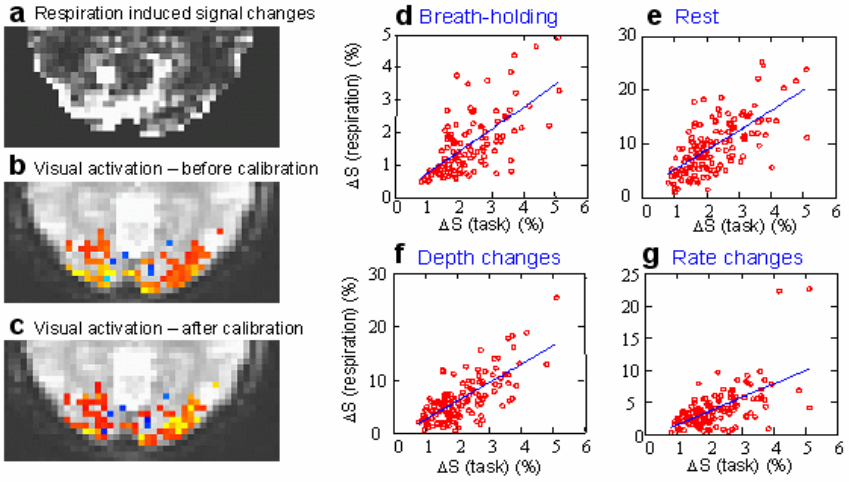


**Figure 16: a. Respiration induced signal changes during rest. b. Visual activation (before calibration). c. Visual activation after calibration using respiration fluctuations during rest as the calibrating signal. d-g. Correlation between task-induced and respiration-induced signal changes for active voxel in visual cortex. In this subject, breath-holding changes appear weakest, relative to the other calibration signals.**

## 2C-2. Better understanding of the respiration response function

Work by our group (section 1B-3 and 1B-4) and others [21] have shown that variations in the rate and depth of breathing can cause significant fMRI signal changes. These changes are particularly problematic for functional connectivity analyses, a technique that infers the connections of neuronal networks by measuring the correlation of low frequency (<0.1 Hz) BOLD-fMRI signal fluctuations between and within brain regions. Respiration induced signal changes can occur in similar brain regions and at similar low frequencies. In order to obtain resting-state activity maps that reflect fluctuations in neuronal activity exclusively, it is vital that these respiration-induced fluctuations are modeled or removed from the data.

Regressing out a time-shifted estimate of the changes in respiration volume per time (RVT) resulted in no significant difference in estimates of functional connectivity (section 1B-3). This is likely due to the fact that a sudden respiration change results in a relatively slow MR signal change (section 1B-4). Modeling the respiration-induced signal change using the respiration response function derived from a single deep breath, however, has two additional complications. First, the respiration induced signal changes during rest appear to be slightly faster than the respiration induced signal changes during cued breathing variations, as shown in Figure 17. Second, the respiration response function appears to vary across the brain, as shown in Figure 18. Future studies will investigate the temporal dynamics and spatial heterogeneity of signal changes induced by variations in breathing during rest. These dynamics and spatial heterogeneity may also reflect baseline physiological information, of relevance both to the BOLD response and to more general physiologic abnormalities

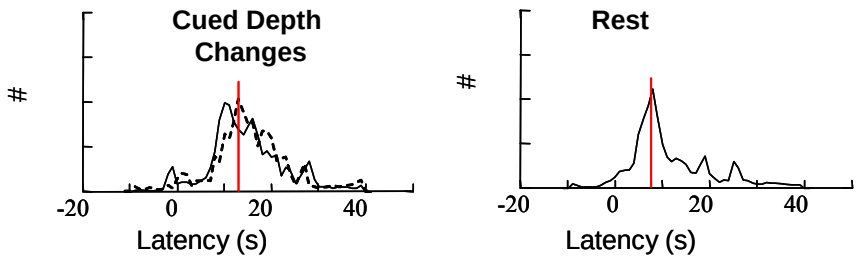


**Figure 17: Histograms (across voxels) of the optimal latency for fitting the RVT time course to the fMRI signal in each voxel. Left: cued depth changes Right: resting fluctuations in breathing. Note that respiration induced signal changes (correlated with RVT) are faster during rest.**

Future work will also investigate the effect of respiration changes on 1) functional connectivity estimates derived from independent component analysis; and 2) functional connectivity maps obtained during external stimuli or task performance, rather than during the resting state.

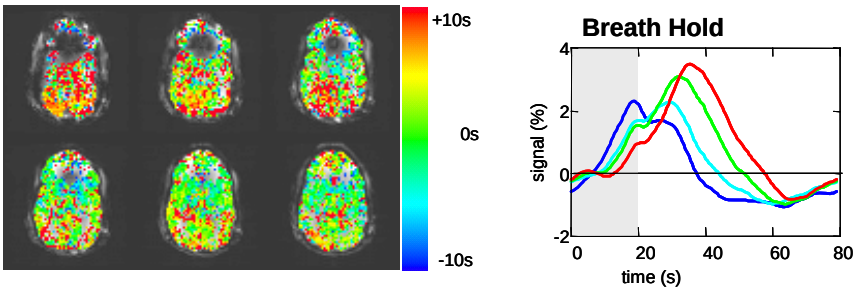


**Figure 18: Left: Maps showing the latency of the respiration induced response (relative to the average RVT*RRF) for each voxel in one subject Right: average signal intensity time courses for voxels with the optimal latency within four ranges: (-10s to -5s, -5s to 0s, 0s to 5s, and 5s to 10s).**

The spatial overlap between respiration-induced signal changes and the default mode network raises the interesting possibility of a closer link between respiration variations and neuronal activity. This will be investigated by simultaneously measuring the respirations and neuronal activity during rest using MEG. An estimate of the RVT will be correlated with the MEG power in various frequency bands, as well as the total MEG power. A significant correlation will indicate that respiration induced fMRI signal changes reflect, at least in part, true underlying changes in neuronal activity. (**Birn**, Handwerker, Jones)

### 2C-3. Validation of BOLD response variability calibration

In a current study (section 2C-1), we have shown that the relative amplitude of the activation-induced fMRI response across the brain can be calibrated using either spontaneous fluctuations in breathing, or various cued breathing manipulations. The accuracy of this calibration, both across the brain and across subjects, has not yet been fully determined. In this study, we will address two questions: a) Does respiration based calibration improve the BOLD amplitude estimate? and b) Does respiration based calibration improve localization of function? To address the first question, we will use a well controlled stimulus such as alternating visual hemifield activation to modulate relative intensity of activation. To address the second question, we will use other "gold standard" functional localization techniques such as perfusion imaging, combined with accurate venograms to mask large vessel effects and compare these maps to the calibrated maps. Extending this technique to calibrate the BOLD response across subject will require two additional steps: 1) accounting for the actual amount that each subject varies his or her own breathing, and 2) accounting for a possible variation in the respiration response function across subjects. (**Birn**, Handwerker, Jones)

## Theme 3: Technology

### 3A. Introduction: practical advances

SFIM has worked with FMRIF over the past four years to develop technology aimed not only at furthering applications but also in enhancing the ability to ask deeper questions related to interpretation of the fMRI signal. In the past, collaboration of SFIM and FMRIF has resulted in pulse sequence developments and hardware developments. Recently, we have been collaborating with FMRIF and Bob Cox's group, the Statistical and

Scientific Computing Core facility (SSCC) to further advance real time measurement of fMRI signal well as real time complementary signals such as respiration, cardiac function, and other neurophysiologic measures. We have also been collaborating with Carlo Porro from Udine, Italy on spinal cord imaging, and have designed a spinal cord coil (constructed by Nova Medical) for this work. It is mentioned in the applications section.

While we have scaled back our efforts on neuronal current imaging we have not stopped it. We have a neuronal current imaging study in progress involving the implementation of an adaptive filter methodology developed with electroencephalogram (EEG) methodology.

Two papers highlighted in the progress report are a paper about neuronal current imaging in cell cultures as well as a paper that demonstrates the temporal signal to noise advantage of going to smaller voxel volumes.

## 3B. Progress Report

### 3B-1: Neuronal current imaging of cell cultures

Recent studies have shown evidence (phantom, animal, and human data) that MRI may be used to directly and noninvasively map electrical activity associated with brain activation [22-26]. Here, we show that MRI can detect changes that related to neuronal activity in blood free samples[27]. We use rat brain cultures *in vitro* that are spontaneously active in the absence of a cerebrovascular system – thus avoiding BOLD contamination. Single-voxel MR measurements obtained at 7 T showed correlation with multisite extracellular local field potential recordings of the same cultures before [PRE] and after blockade of neuronal activity with tetrodotoxin [TTX]. Similarly, for MR images obtained at 3 T, the MR showed changes only in voxels containing the culture.

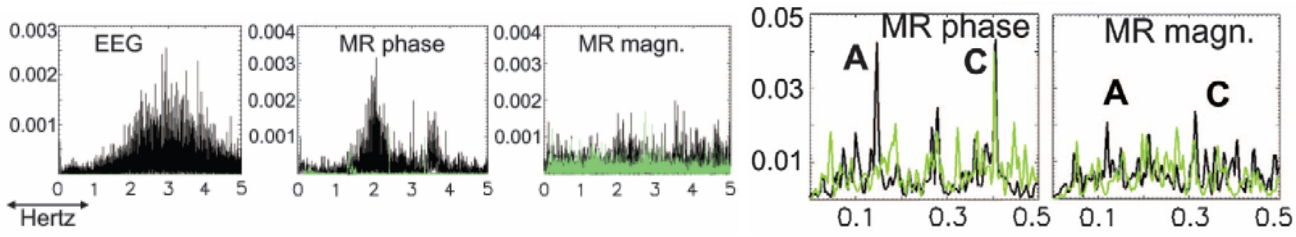


**Figure 19: a. EEG and 7T FID data. EEG and MR power spectrum of cell culture phase and magnitude before (black) and after (green) administration of TTX, a sodium channel blocker. Clear reduction of EEG, phase, and even magnitude power is seen after TTX administration. b. 3T MRI data showing reduction in specific spectral peaks with administration of TTX. In the figure A, is the frequency of interest. C is the frequency of the cryogen pump on the scanner.**

Two sets of experiments were performed. The results are shown in Figure 19. In the first experiment, MR measurements were obtained by using a 7T MR scanner and a free induction decay (FID) technique allowing high temporal resolution and sensitivity. The cultures were grown on 60-channel multielectrode arrays (MEA) allowing for multisite local field potential (LFP) recordings[28] before and after the MR sessions. MR signals were acquired every 100 ms, and were obtained from a single volume (40 $mm^3$) that encompassed the culture. EEG measurements were obtained immediately before and after each MR session, which corresponded to the PRE and TTX states for the given culture. Power spectra were obtained from the EEG and MR time series for the PRE and TTX states. The spectra were compared between the two states to identify decreases in signal power that would indicate the suppression of MR signal variation after TTX infusion. These recordings were compared with MR measurements obtained from each culture. Correlation between signal power changes at the culture activation frequency range, obtained with both techniques, would be evidence that neuronal activity was directly detectable by MR. The second experiment was performed by using a 3-T MR scanner with a conventional imaging technique and no electrical recordings.

The EEG data sets showed a decrease in signal power in the TTX state as compared with the PRE state (power decrease: 83.6 $\pm$ 19.4%). The corresponding MR data sets also showed a decrease in the signal power in the

TTX state as compared with the PRE state; however, the effect was more pronounced for MR phase than for MR magnitude (power decrease 57.6 $\pm$ 24.5% and 12.4 $\pm$ 10.2%, respectively). The three EEG wash data sets showed the recovery of spontaneous neuronal activity in the cultures (wash signal power increase: 94.6 $\pm$ 2.5%) When including all seven cultures for the MR data analysis, similar results were obtained (PRE vs. TTX signal power decrease for MR phase 60.5 $\pm$ 21.5% and for MR magnitude 18.8 $\pm$ 16.3%). (Bodurka, **Petridou**, Plenz, Silva)

### 3B-2: High resolution improves fMRI quality in anterior MTL regions.

A straightforward solution to correct for susceptibility-related signal dropout is to reduce intra-voxel dephasing and intravoxel tissue heterogeneity by reducing voxel size, especially in the slice (z) direction [29, 30]. However, because signal is proportional to voxel volume, decreasing slice thickness reduces signal-to-noise ratio (SNR) [29]. One solution to this problem is to acquire alternating thin slices on consecutive volumes and add these adjacent slices to recover lost SNR. Though this approach reduces signal dropout and may recover SNR, the gains in spatial and temporal resolution are limited.

Recent advances in MRI receiver and coil technologies have led to the development of multi-element receive-only surface coil arrays, suitable for whole brain imaging, that enhance SNR [31]. The 16-element array coil used in this report offers an overall 3-fold SNR improvement over a standard birdcage head coil during EPI acquisition [32]. We evaluated the effect of increasing fMRI spatial resolution by reducing slice thickness to determine if this would help to recover signal from regions containing anterior medial temporal lobe (MTL) [33]. We predicted that, at higher EPI resolution (thinner slices), the gain in image SNR would translate to improved EPI image-to-image stability (TSNR) and enhanced BOLD signal detection (CNR). However, the cost of reducing voxel volume is a reduction in the imaging volume coverage per unit time.

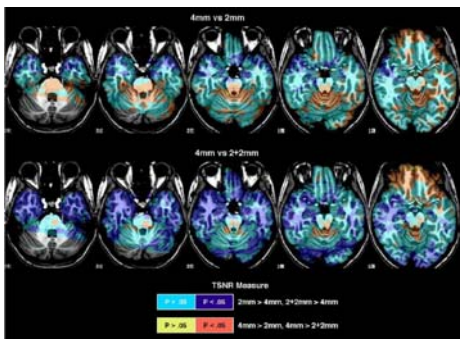


**a**

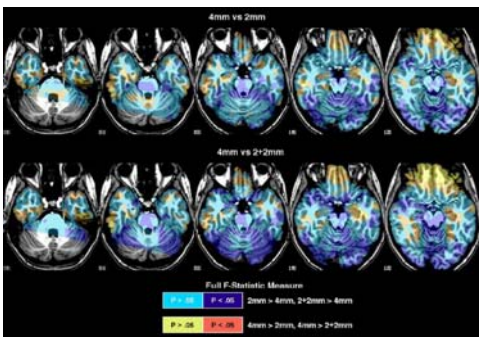


**b**

**Figure 20. Temporal a. signal to noise and b. contrast to noise comparison between 2mm and 4mm (upper row) and 2+2 mm and 4mm (lower row) thick slices. Cool colors represent areas showing greater TSNR for 2 mm and 2 + 2 mm thick slices, and warm colors represent greater TSNR for the 4 mm slices.**

Animal electrophysiological and human lesions studies have implicated anterior medial temporal and frontal regions as critically involved such cognitive tasks as declarative memory function, reinforcement evaluation and executive control. Studies of these regions have been limited due to MR imaging artifacts that are particularly prominent in these regions. The relationships among signal-to-noise, slice thickness, and contrast-to-noise were experimentally investigated at 3 T using memory tasks known to activate MTL regions. Figure 20 shows that the greatest TSNR and TCNR increases are located in brain areas most sensitive to susceptibility artifacts.

Thinner slices combined with higher coil sensitivity improved TSNR and TCNR throughout the ventral medial and lateral regions of the MTL, anterior temporal lobe and ventral orbital frontal gyrus. The improvement in TSNR using thinner slices was associated with decreased intra-voxel MR signal dephasing by suppression of exogenous magnetic field gradients effects at tissue interfaces. Improvements in CNR related to slice thickness reduction may involve interplay among the MR intensity, susceptibility artifacts, physiological noise reduction, and intravoxel tissue heterogeneity. The advances in the MRI receiver and reception array coil technologies offer new possibilities for robust high resolution and high field functional studies of MTL. (**Bellgowan**, Bodurka, Martin, Van Gelderen)

## 3C. Current and Future Experiments

### 3C-1. Perfusion measurements: proportionality to gray matter and comparison

Because most grey matter (GM) voxels are generally not fully occupied by GM, the calculated perfusion is likely to be underestimated. At a high enough spatial resolution, the measured perfusion values should plateau, but they don't – suggesting a much finer structure. We have implemented a double inversion recovery pulse sequence to null out CSF and WM signal in order to estimate the fractional volume of GM and compare with absolute perfusion measurements from Pulsed Arterial Spin Labeling (PASL) techniques. With a typical GM ROI, selected by T1, the average cerebral blood flow (CBF) is 100 ml/100 g/min and the average GM volume fraction is on the order of 55% at current resolution with a voxel size about 100mm$^3$. This is consistent with PET studies which report about 50 ml/100 g/min in which the voxel size is on the order of 200mm$^3$. This implies that perfusion can reach 200 ml/100 g/min in pure GM voxels.

Continuous ASL (CASL) creates tagged blood in finite space and utilizes time for building up the width of the tag whereas PASL inverts the spins in a finite time period and relies on available physical space to create the tag. Both techniques allow for quantitative estimation of CBF by incorporating a post-labeling delay. Additionally, Dynamic susceptibility contrast (DSC) MR imaging provide a simple way to estimate relative CBF (rCBF) as well as relative cerebral blood volume with high SNR using widely available pulse sequences.

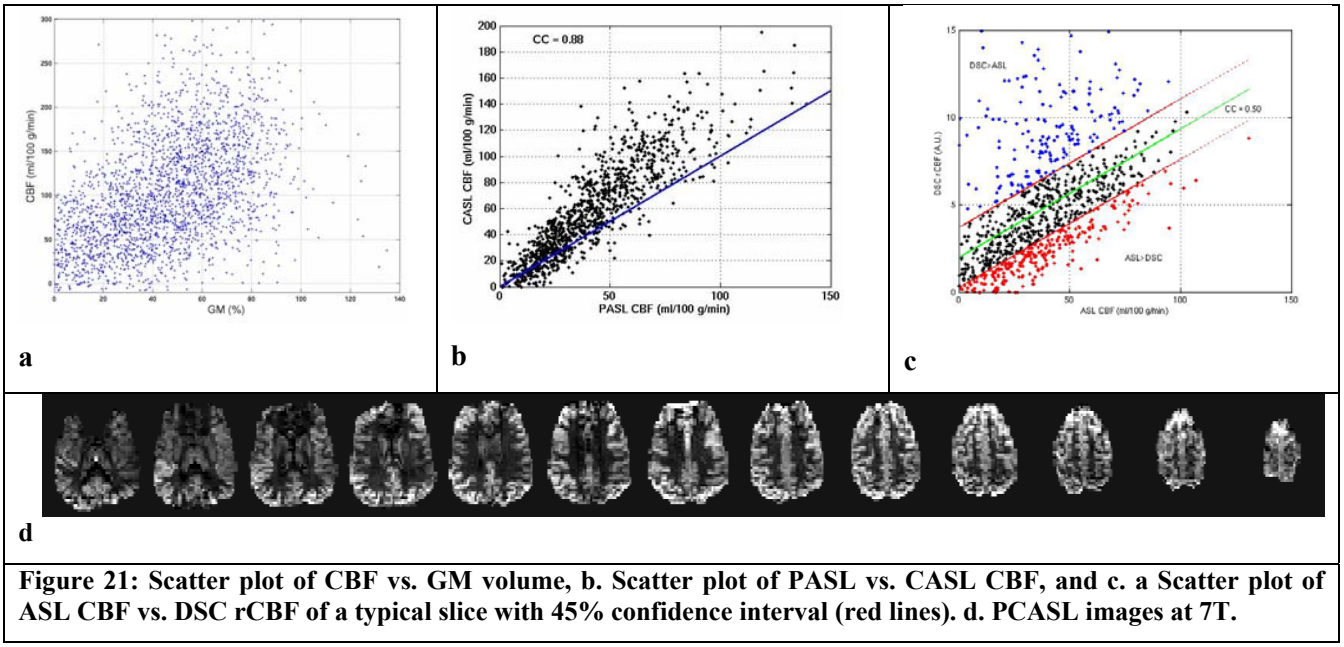


**Figure 21: Scatter plot of CBF vs. GM volume, b. Scatter plot of PASL vs. CASL CBF, and c. a Scatter plot of ASL CBF vs. DSC rCBF of a typical slice with 45% confidence interval (red lines). d. PCASL images at 7T.**

A direct voxel-wise comparison study of QUIPSS II and CASL using a separate labeling coil at 3T was performed as well as comparison between QUIPSS II and DSC. The data comparisons are summarized in Figure 21a-c. CASL and PASL data show a high correlation (CC=0.81) although PASL shows a trend of decreasing CBF toward distal slices probably due to imperfect slice profile effects. Partial volume averaging with CSF and WM would cause overestimation and underestimation of GM, respectively. DSC images show high rCBF values at voxels containing what are likely arteries. DSC data shows more widely distributed rCBF values at high T1 voxels, which is not typically observed with ASL. The correlation coefficients between ASL and DSC data are 0.45, 0.43, and 0.31 in the 5-slice volume, GM, and WM ROIs, respectively. In the low flow voxels, ASL shows slightly lower values than DSC. This is likely due to underestimation of WM perfusion with PASL whereas in the high flow voxels, DSC shows more voxels with higher values than ASL. In voxels where DSC is much greater than ASL, the mean T1 deviates further from the regression line, suggesting that these contain larger vessels surrounded by CSF. Voxels where ASL>DSC, the constant T1 suggests an even mix of GM and WM.

Pseudo-continuous Arterial Spin Labeling (PCASL) allows for direct control of the tag duration, as in CASL, and can be performed with standard commercial scanners. The labeling period for optimal SNR efficiency increases with blood T1 and therefore field strength. We have implemented PCASL and have experimentally

determined that an approximately 3 sec labeling period is required for whole brain perfusion measurements at 3T. For whole brain PASL at higher field strength, a longer than 1sec tag may not be feasible due to limited body RF/gradient coil size and fast flowing blood in labeling arteries. We have designed and implemented a version of PCASL with variable-rate selective excitation resulting in a 20% reduction in SAR. The reduction in SAR permits the application of PCASL at higher field strengths, allowing for longer labeling periods. Figure 21d shows the 7T PCASL images. (Kao, **Luh,** Talagala, Wong)

## Theme 4: Applications

### 4A. Introduction: Carrying Themes 1 - 3 through to Theme 4.

Applications of fMRI that come out of SFIM are those that best utilize Themes 1 through 3 and the available technical expertise in SFIM and FMRIF. In the past four years, some exciting applications have been a direct result of advances in interpretation and methodology from SFIM. As an example, the application in 4B-1 (Imaging subjects during a continuous speaking task) directly utilizes the techniques developed in 2B-2. The concepts of multivariate analyses developed in 2B-6 and 2C-5 are brought to bear in a novel and exciting manner in 4B-3 (Man & Monkey IT comparison). Lastly, the spinal coil that was developed in SFIM was used for functional MRI of the human spinal cord in 4B-2.

Several applications that were carried out in SFIM are not mentioned in this report due to space limitations. Specifically, studies related to fear conditioning by David Knight and his post bac IRTA, Joey Dunsmoor, are not included, and studies involving decision making and auditory processing carried out by Anthony Boemio are not mentioned.

### 4B. Progress Report

#### 4B-1. BOLD fMRI of the human spinal cord during willed motor actions

Although the spinal cord is the output station of the central motor system, little is known about the relationships between its functional activity and willed movement parameters in humans. We investigated BOLD signal changes in the cervical spinal cord during a simple finger-to-thumb opposition task in thirteen right-handed volunteers, using a dedicated array of 16 receive only surface coil (developed through a collaboration between SFIM and Nova Medical, Inc.) on a 3T MRI system [34]. In a first experiment, shown in Figure 26a, we found significant fMRI signal increases on both sides of the lower cervical spinal cord while subjects performed the motor task at a comfortable pace (~0.5 Hz), using either hand. Both the spatial extent of movement-related clusters, and peak signal increases were significantly higher on the side of the cord ipsilateral to the moving hand than on the contralateral side. Movement-related activity was consistently larger than signal fluctuations during rest.

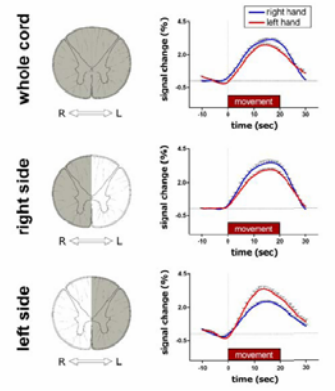


a.

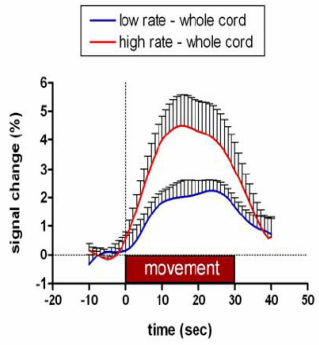


b.

**Figure 26: a. Filtered (mean ± S.E.M.) time courses of fMRI signal changes from baseline, averaged around the movement ("perimovement plots") in the whole spinal cord (*top*), the right side of the spinal cord (*middle*) and the left side of the spinal cord (*bottom*). b. Filtered time courses of fMRI signals averaged around the movement ("peri-movement plots") during movements of the right hand at "low" or "high" frequency.**

In a second experiment, shown in Figure 26b, we recorded spinal cord responses while the same motor sequence was performed using the dominant hand at two different rates (~ 0.5 Hz or 1 Hz). The intensity, but not the spatial extent of the response was larger during higher rates, and it was higher on the ipsilateral side of the cord.

Notwithstanding the limited spatial resolving power of the adopted technique, the present results clearly indicate that the finger movement-related fMRI signals recorded from the spinal cord have a neural origin and that due to recent technological advances fMRI can be used to obtain novel and quantitative physiological information on the activity of spinal circuits. (Bodurka, Iannetti, **Maieron**, Porro, Tracy).

## 4C. Current and Future Experiments

### 4C-1. A self-paced overt response fMRI study

Verbal fluency tasks are commonly used in neuropsychological tests to evaluate language abilities and the cognitive function of executive control. These tasks require subjects to generate lists of words that begin with a specific letter (orthographic or phonemic fluency) or belong to a specific conceptual category (semantic fluency). Behavioral and lesion studies have suggested that these two fluency tasks place differential demands on retrieval strategy and conceptual knowledge, and, as a result, place differential demands on frontal and temporal lobe processes. Previous fMRI studies of verbal fluency have typically used covert word processing or cued single word production in order to avoid motion artifacts. A key element of tests of executive function in verbal fluency, however, is the efficiency of accessing and retrieving semantic and phonemic information, which becomes evident when trying to generate multiple words as quickly as possible.

In this study, we used a novel experimental design, consisting of 10s periods of task performance alternated with 10s of rest, in order to minimize the task-induced motion artifacts and maximize the detection of true function. Activations during the fluency task were observed in anterior and superior left frontal gyrus, left inferior frontal gyrus (IFG), bilateral precentral gyrus, left fusiform, and bilateral parietal and occipital cortices. Figure 25 shows that, in agreement with our prediction, left IFG was more active for phonemic fluency, while anterior and superior left frontal gyrus, and left fusiform gyrus (areas typically involved in conceptual processing) were more active for category fluency. Signal changes synchronous with the task, indicative of task-related motion, were located primarily in inferior temporal and orbito-frontal regions and were not significantly correlated with the delayed BOLD response. Activation maps with minimal task-related motion artifact can therefore be produced during a self-paced overt speech task using the proper experimental timing. Furthermore, these findings provide converging evidence suggesting that letter and category fluency performance is dependent on partially distinct neural circuitry. (**Birn**, Caravella, Case, Jones, Kenworthy, Martin)

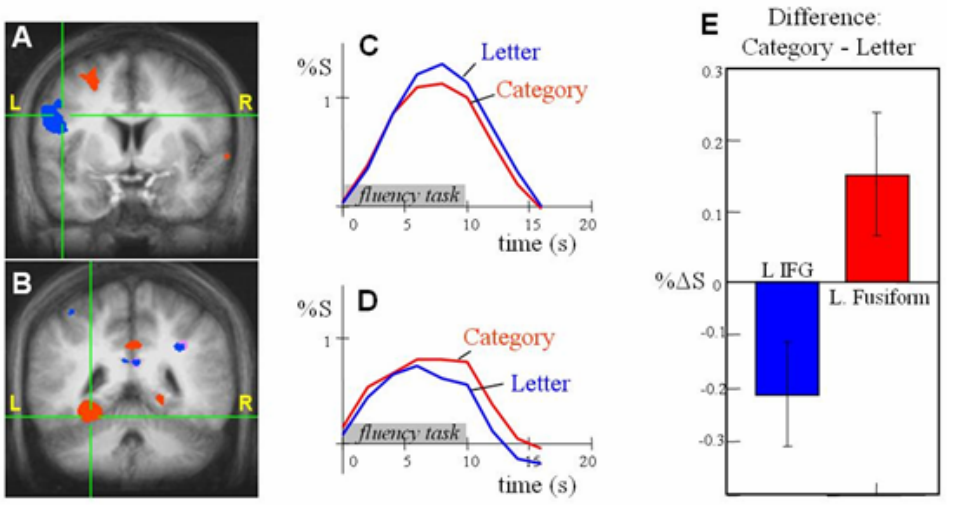


**Figure 25: Activation during semantic (category) and phonemic (letter) fluency in a. left inferior frontal gyrus and b. left fusiform gyrus. Red regions represent greater activation during semantic fluency, blue regions represent greater activation during phonemic fluency. c-d. averaged fMRI time courses from left IFG and left fusiform, respectively. e. Differences in activation amplitude between category and letter fluency in the left IFG and fusiform.**

### 4C-2. Matching IT representation in man and monkey: comparing single-cell recording and fMRI.

Monkey single-cell recordings have shown that primate inferotemporal (IT) neurons respond selectively to visual features occurring in natural images as parts of objects. A recent study has demonstrated that monkey-IT response patterns cluster according to natural categories[35]. Human neuroimaging has demonstrated conventional-category information in human IT cortex (in both focal activations and widely distributed response patterns). However, a focus on category-average responses has precluded addressing if a categorical structure is inherent to the representations and, if so, what the natural categories are.

This study combines human and monkey data from hi-res fMRI and single-cell recordings, respectively. We investigate response patterns elicited by the same 92 photographs of isolated natural objects in IT cortex of both species. Each stimulus image forms an independent condition. No predefined stimulus grouping is implied in either the experimental design or the core analyses to be applied. Because response patterns are difficult align between species or even among human subjects, we relate monkey and human representations by considering, for each pair of stimuli, the similarity of the response patterns the two stimuli elicit. This approach also allows us to relate both species to computational models exposed to the same stimuli.

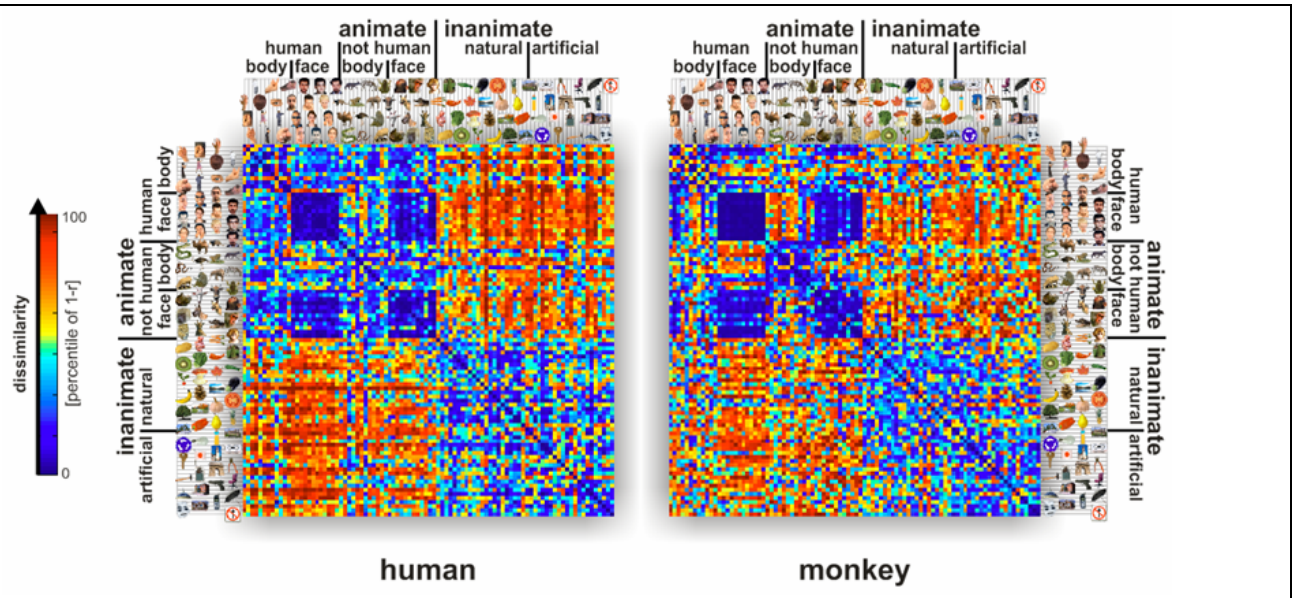


**Figure 27: IT response-pattern dissimilarity matrices. For each pair of stimuli, each matrix (human, monkey) color codes the dissimilarity of the two response patterns elicited by the stimuli in IT. The dissimilarity measure is 1-r (Pearson correlation across space). The matrices have been separately histogram-equalized (percentile units) for easier comparison. The two matrices are the product of completely separate experiments and analysis pipelines (data not selected to match). Human data is from 316 bilateral inferotemporal voxels (1.95×1.95×2 mm$^3$) with the greatest visual response in an independent data set. Dissimilarity matrices averaged across 2 sessions for each of 4 subjects. Monkey data is from >600 IT single cells isolated in two monkeys.**

Monkeys performed a fixation task while presented with the images in rapid succession [35]. Responses of more than 600 cells were recorded in two monkeys (right and left anterior IT cortex, respectively). Human subjects detected color changes occurring at fixation during image presentation while we measured response patterns with hires fMRI (3T, SENSE, voxels: 1.95x1.95x2mm$^3$).

Primate IT response patterns across these two species cluster in natural categories, with the animate-inanimate distinction explaining most variance and faces forming a very focused subcluster. Human-fMRI early visual response patterns and several low-level representations of the images (luminance pattern, color pattern, silhouette pattern, V1 model representation) exhibit no category clustering. We suspect that a computational model accounting for our results would need to have complex statistical category knowledge as might be acquired by supervised learning. Our results suggest that the extraction of information on membership in these behaviorally crucial categories constitutes a fundamental function of primate IT across species. Within the

category clusters, the primate IT code appears to represent more fine-grained object information. This information as well is consistent across species and may reflect a form of visual similarity. The close match provides some hope that data from single-cell recording and fMRI, for all their differences, may consistently reveal neuronal representations when subjected to massively multivariate analyses of response-pattern information. (Bodurka, Esteky, Kiani, **Kriegeskorte**, Mur, Ruff, Tanaka)

## Conclusion

The work of this section is diverse yet integrated. There are several overriding objectives that are apparent throughout this report. The first is the effort to "squeeze" as much meaningful information as possible from the fMRI time series in as an efficient and complete manner as possible. The second is to develop powerful, innovative, yet practical tools for those who desire to perform fMRI at high resolution.

Post docs including Anthony Boemio and David Knight have been performing highly innovative "application" research on auditory processing and fear conditioning respectively, that has benefited from being generated in this methods-focused environment. Other projects have also not been mentioned, including those from several students and post-bac IRTAs including Joey Dunsmoor, Tyler Jones, Marieke Mur, Doug Ruff, and Monica Smith. SFIM has been extremely successful in fostering independence in these students and post-bac IRTAs. They typically start independent projects within a year of arriving in SFIM. These post-bac IRTA projects, with the exception of Tyler Jones', have focused on applications and remain central to the approach that SFIM fosters: multidisciplinary and aware not only of the technical and methodological limits of fMRI, but of the unique potential that fMRI offers. This approach is beneficial to methodologists and application specialists alike.

We have also maintained our collaboration with the other sections in the Laboratory of Brain and Cognition. We continue to collaborate with Leslie Ungerleider with regard to the fMRI of decision making project and are starting an excellent collaboration with Alex Martin with regard to his autism project.

In the future, we look forward to shifting much of our methods, interpretation, and applications work to the 7T, dealing with the challenges it presents, making use of the clear advantages in sensitivity and contrast that it offers, and also exploring the potentially new types of functional and anatomical contrast that may be revealed.

## Acknowledgements

I would like to thank the past and present members of SFIM and FMRIF who have contributed their work and/or edits to this report. These include: Rasmus Birn, Jerzy Bodurka, Anthony Boemio, Joey Dunsmoor, Javier Gonzales-Castillo, Tyler Jones, Youn Kim, David Knight, Niko Kriegeskorte, Wenming Luh, Marta Maieron, Sean Marrett, Marieke Mur, Kevin Murphy, Doug Ruff, Monica Smith, August Tuan. I would also like to thank Kay Kuhns and Dorian Van Tassell for their assistance in preparation of summary materials–and practically every administrative need in SFIM and FMRIF.

## References

1. Birn, R.M., et al., *The effect of stimulus duty cycle and "off" duration on BOLD response linearity.* Neuroimage, 2005. **27**(1): p. 70-82.
2. Mandeville, J.B., et al., *Evidence of a cerebrovascular postarteriole windkessel with delayed compliance.* Journal of Cerebral Blood Flow and Metabolism, 1999. **19**(6): p. 679-689.
3. Buxton, R.B., et al., *Modeling the hemodynamic response to brain activation.* Neuroimage, 2004. **23**: p. S220-S233.
4. Birn, R.M., et al., *Separating respiratory-variation-related fluctuations from neuronal-activity-related fluctuations in fMRI.* NeuroImage, 2006. **31**(4): p. 1536-1548.
5. Glover, G.H., et al., *Image-based method for retrospective correction of physiological motion effects in fMRI: RETROICOR.* Magnetic Resonance in Medicine, 2000. **44**(1): p. 162-167.

6. Goelman, G., *Radial correlation contrast - A functional connectivity MRI contrast to map changes in local neuronal communication.* NeuroImage, 2004. **23**(4): p. 1432-1439.
7. Kruger, G., et al., *Physiological noise in oxygenation-sensitive magnetic resonance imaging.* Magnetic Resonance in Medicine, 2001. **46**(4): p. 631-637.
8. Rees, G., et al., *A direct quantitative relationship between the functional properties of human and macaque V5.* Nature Neuroscience, 2000. **3**(7): p. 716-723.
9. Braddick, O.J., et al., *Form and motion coherence activate independent, but not dorsal/ventral segregated, networks in the human brain.* Current Biology, 2000. **10**(12): p. 731-734.
10. McKeefry, D.J., et al., *Mapping and topographic organization of the visual field in human area V4 as revealed by fMRI.* Neuroimage, 1997. **5**(4): p. S1-S36.
11. Paradis, A.L., et al., *Visual perception of motion and 3-D structure from motion: an fMRI study.* Cerebral Cortex, 2000. **10**(8): p. 772-783.
12. Rainer, G., et al., *Nonmonotonic noise tuning of BOLD fMRI signal to natural images in the visual cortex of the anesthetized monkey.* Current Biology, 2001. **11**(11): p. 846-854.
13. Kriegeskorte, N., et al., *Analyzing for information, not activation, to exploit high-resolution fMRI.* NeuroImage, in press.
14. Kriegeskorte, N., et al., *Information-based functional brain mapping.* Proceedings of the National Academy of Sciences of the United States of America, 2006. **103**(10): p. 3863-3868.
15. Bodurka, J., et al., *Mapping the MRI voxel volume in which thermal noise matches physiological noise-Implications for fMRI.* NeuroImage, 2007. **34**(2): p. 542-549.
16. Birn, R.M., et al., *Experimental designs and processing strategies for fMRI studies involving overt verbal responses.* Neuroimage, 2004. **23**(3): p. 1046-1058.
17. Murphy, K., et al., *How long to scan? The relationship between fMRI temporal signal to noise ratio and necessary scan duration.* NeuroImage, 2007. **34**(2): p. 565-574.
18. Davis, T.L., et al., *Calibrated functional MRI: Mapping the dynamics of oxidative metabolism.* Proceedings of the National Academy of Sciences of the United States of America, 1998. **95**(4): p. 1834-1839.
19. Bandettini, P.A., et al., *A hypercapnia-based normalization method for improved spatial localization of human brain activation with fMRI.* Nmr in Biomedicine, 1997. **10**(4-5): p. 197-203.
20. Thomason, M.E., et al., *Calibration of BOLD fMRI using breath holding reduces group variance during a cognitive task.* Human Brain Mapping, 2007. **28**(1): p. 59-68.
21. Wise, R.G., et al., *Dynamic forcing of end-tidal carbon dioxide and oxygen applied to functional magnetic resonance imaging.* Journal of Cerebral Blood Flow and Metabolism, 2007. **27**(8): p. 1521-1532.
22. Park, T.S., et al., *Effect of nerve cell currents on MRI images in snail ganglia.* Neuroreport, 2004. **15**(18): p. 2783-2786.
23. Kraus Jr, R.H., et al., *Toward SQUID-based direct measurement of neural currents by nuclear magnetic resonance.* IEEE Transactions on Applied Superconductivity, 2007. **17**(2): p. 854-857.
24. Truong, T.K., et al., *Finding neuroelectric activity under magnetic-field oscillations (NAMO) with magnetic resonance imaging in vivo.* Proceedings of the National Academy of Sciences of the United States of America, 2006. **103**(33): p. 12598-12601.
25. Xiong, J., et al., *Directly mapping magnetic field effects of neuronal activity by magnetic resonance imaging.* Human Brain Mapping, 2003. **20**(1): p. 41-49.
26. Bodurka, J., et al., *Toward direct mapping of neuronal activity: MRI detection of ultraweak, transient magnetic field changes.* Magnetic Resonance in Medicine, 2002. **47**(6): p. 1052-1058.
27. Petridou, N., et al., *Direct magnetic resonance detection of neuronal electrical activity.* Proceedings of the National Academy of Sciences of the United States of America, 2006. **103**(43): p. 16015-16020.
28. Beggs, J.M., et al., *Neuronal Avalanches in Neocortical Circuits.* Journal of Neuroscience, 2003. **23**(35): p. 11167-11177.
29. Merboldt, K.D., et al., *Reducing inhomogeneity artifacts in functional MRI of human brain activation - Thin sections vs gradient compensation.* Journal of Magnetic Resonance, 2000. **145**(2): p. 184-191.
30. Wadghiri, Y.Z., et al., *Sensitivity and performance time in MRI dephasing artifact reduction methods.* Magnetic Resonance in Medicine, 2001. **45**(3): p. 470-476.

31. Bodurka, J., et al., *Scalable multichannel MRI data acquisition system.* Magnetic Resonance in Medicine, 2004. **51**(1): p. 165-171.
32. De Zwart, J.A., et al., *Signal-to-Noise Ratio and Parallel Imaging Performance of a 16-Channel Receive-only Brain Coil Array at 3.0 Tesla.* Magnetic Resonance in Medicine, 2004. **51**(1): p. 22-26.
33. Bellgowan, P.S.F., et al., *Improved BOLD detection in the medial temporal region using parallel imaging and voxel volume reduction.* NeuroImage, 2006. **29**(4): p. 1244-1251.
34. Maieron, M., et al., *Functional responses in the human spinal cord during willed motor actions: Evidence for side- and rate-dependent activity.* Journal of Neuroscience, 2007. **27**(15): p. 4182-4190.
35. Kiani, R., et al., *Object category structure in response patterns of neuronal population in monkey inferior temporal cortex.* Journal of Neurophysiology, 2007. **97**(6): p. 4296-4309.